

Effects of Pore Fluids and Sand Particles on Electrochemical Characteristics of Sandy Soil Containing Soluble Sodium Salt

Ruizhen Xie^{1,2}, Pengju Han^{2,*}, Xiaoyuan Wang², Boqiong Li¹, Bin He², Fuli Ma² and Xiaohong Bai²

¹ Mechanics Institute, Jinzhong University, Jinzhong 030619, China

² Department of Civil Engineering, Taiyuan University of Technology, Taiyuan 030024, China

*E-mail: 13834569544@163.com

Received: 2 December 2019 / Accepted: 19 January 2020 / Published: 10 March 2020

The electrochemical impedance spectroscopy (EIS) characteristics of sandy soil and pore fluids containing different concentrations of NaCl, Na₂SO₄ or NaHCO₃ were tested and comprehensively analysed. The equivalent circuit fitting and analysis results show that the basic equivalent circuit of the sandy soil system is circuit ① R(C(R(Q(RW))))). The EIS of different sandy soils show their respective characteristics. Compared with those of the pore fluids, the radius of the capacitive loop and the peak of phase angle for the sandy soil is small, showing the high corrosivity of sandy soil. The sand particles facilitate low-frequency processes and hinder high-frequency processes. In the high-frequency region, the three conductive paths in the sandy soil are mostly in the conducting state, and the corresponding modulus is large. At the frequencies of 10⁰~10² Hz, the peak of phase angle for the sandy soil containing NaCl, Na₂SO₄ or NaHCO₃ is greatly affected by the concentration of the pore fluid, which may be caused by the porous structure and the state of the "liquid bridge".

Keywords: EIS, sandy soil, corrosivity, equivalent circuit

1. INTRODUCTION

Soil corrosivity is an indispensable parameter for engineering designs, such as pipeline laying, grounding designs (power systems), and bridge structures [1-5]. Foreign studies in this area are in relatively early stages, and research on the corrosion of materials in China's natural environment (atmosphere, seawater, soil) began in the 1950s [6]. At present, China has initially established a natural environmental corrosion test network (Figure 1) that has guided a large number of engineering applications. However, a material corrosion test station has not been established in Shanxi Province. Therefore, basic theoretical research on the electrochemical properties and corrosion mechanism of the soil in Shanxi Province has important scientific significance and application value.

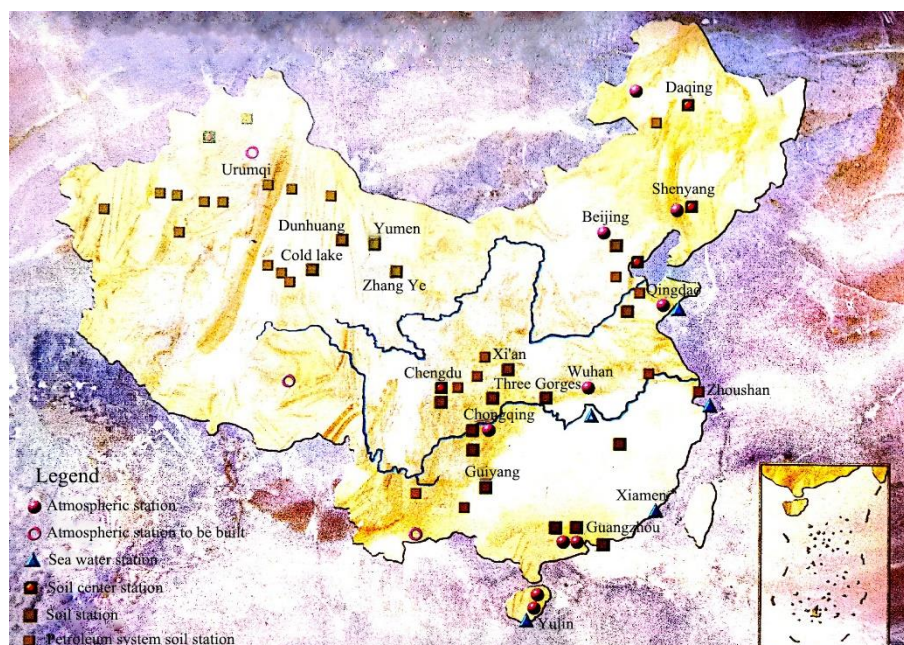


Figure 1. Distribution of the soil corrosion test stations in China[6]

The pollution mechanism of contaminated soil mainly focuses on the ion exchange, electrical double layer changes and cement dissolution [7, 8]. The formation of polluted soil is a process of conversion, migration, degradation, absorption and diffusion of pollutants in soil-aqueous systems. In an original soil system, a new chemical component is added, or the original chemical composition is changed. The thickness of the electrical double layer is compressed or increased, ultimately affecting the expansion strength of the colloidal particles in the soil, which is macroscopically reflected by the change in the soil engineering properties [9-11]. Clay (kaolinite, illite, and montmorillonite) or clay particles and water or ions experience strong adsorption and exchange, and the electrical double layer affects the permeability of sodium kaolin [12-15]. Research on the engineering properties of contaminated soil is mainly focused on the study of its physical and mechanical properties.

Electrochemical impedance spectroscopy (EIS) principles and testing technology provide new ideas for the application of EIS theory in geotechnical engineering. EIS has been widely used in the research of electrode process dynamics, electrical double layer, electrode materials, solid electrolytes, conductive polymers and corrosion protection. EIS and polarization electrochemical tests have also gradually been applied in research on the electrochemical corrosion of soil environments [16, 17]. EIS and polarization curves can be combined to obtain more soil corrosion information and corrosion kinetic parameters [18]. Electrochemical analysis of a steel/soil interface can be used to estimate the active area of the electrode via the determination of the soil electrolyte resistance and facilitates the monitoring of the evolution of the steel/soil interface [19].

At present, there are many studies on the corrosivity of sandy soil, flourey soil [20, 21] and various contaminated soils [22, 23]; however, the electrochemical properties of sandy soil are still in the preliminary research stage of basic laws and interface theory. Jiang [24] studied the effects of the length, width and liquid film concentration of the three-phase line interface on the oxygen reduction cathode process and corrosion behaviour in sandy soil and found that the length and width of the three-

phase line interface zone have an important impact on the metal corrosion cathode process and corrosion behaviour. Zhang [25] studied the electrochemical impedance characteristics of sandy soil systems with different particle sizes and different water contents and analysed the relationship between circuit parameters and particle size and water content. Ma et al [26-28] analysed the effects of NaCl, Na₂SO₄ and NaHCO₃ on the electrochemical properties of saline sand. He et al [29] systematically studied the effect of soil particle size on the corrosivity of sodium chloride sand by laboratory electrochemical tests. Research on the electrochemical characteristics of sand systems is mainly carried out from two aspects: basic models and equivalent circuit fitting. The research of equivalent circuits needs further exploration.

To further study the co-effects of sand particles and pore fluid containing common soluble sodium salt on the electrochemical characteristics and corrosiveness of sandy soil, the influence of sand particles and pore fluids on the electrochemical behavior and equivalent circuit components of sand soil were revealed, and the influence mechanism of the porous structure on electrochemical conduction process of the sand soil were explored based on the electrochemical theory, soil mechanics and soil adhesion mechanism in this work. The EIS of sandy soil and pore fluid containing a single salt (NaCl, Na₂SO₄, or NaHCO₃ [30]) was carried out under three-electrode systems. The equivalent circuit was selected according to the interface structure of the electrode-sandy soil and the properties of the pore fluid, and the electrochemical behaviour and corrosion of sandy soil containing soluble sodium salt were comprehensively analysed.

2. EXPERIMENTAL METHODS

2.1 Materials

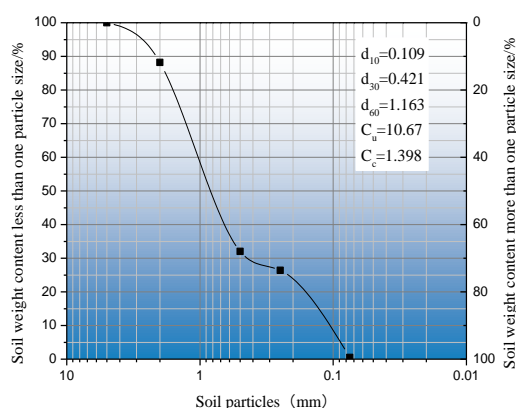


Figure 2. Grain size accumulation curve of the standard sand

To reduce the influence of unrelated variables in sandy soil, the sandy soil used in this work is standard sand manufactured by Xiamen ISO Standard Sand Co., Ltd., and the silica content is greater than 98%. The maximum dry density $\rho_{dmax}=1.86 \text{ g/cm}^3$, the minimum dry density $\rho_{dmin}=1.56 \text{ g/cm}^3$, and the standard sand is dried before use. It can be seen from the grain size accumulation curve of the standard sand that the gradation of standard sand is not continuous, but the conditions of $C_u \geq 5$ and C_c

=1-3 are both satisfied, which indicates that the standard sand is a good grade of coarse sand (Figure 2). The quartz glass cylinder for the test possesses an internal volume of $9.5 \times 9.5 \times 9.5 \text{ cm}^3$, and the water is distilled water. The anions are Cl^- , SO_4^{2-} and HCO_3^- (significantly affecting the soil corrosion), and the cation is Na^+ (the most soluble in water). The salts (NaCl , Na_2SO_4 , NaHCO_3) are all analytically pure reagents.

2.2 Method

In this work, electrochemical impedance spectroscopy (EIS) tests are carried out for sandy soil and pore fluids containing single soluble sodium salts (NaCl , Na_2SO_4 , NaHCO_3). The scheme is shown in Tables 1-2. According to the "Geotechnical Investigation Specification" GB 50021-2001 and the solubility of each soluble salt in water at the test temperature, the concentrations of salt are chosen, where the concentration is the percentage of salt in water. The sample is named for the salt content (%) of the pore fluid in the soil. For example, 0.3% and 0.3%-S refer to a pore fluid with a salt concentration of 0.3% and sandy soil with a pore liquid concentration of 0.3%, respectively.

Table 1. Composition of the sandy soil containing single soluble sodium salt

Sample		$m_{\text{sandy soil/g}}$	$m_{\text{water/g}}$	$m_{\text{salt/g}}$	Liquid content /%	Salt content/%
NaCl (NaCl 58.44 g/mol)	0.3%-S	1000	150	0.45	15.05	0.045
	1.0%-S	1000	150	1.50	15.15	0.150
	3.5%-S	1000	150	5.25	15.53	0.525
	5.0%-S	1000	150	7.50	15.75	0.750
Na ₂ SO ₄ (Na ₂ SO ₄ 142.04 g/mol)	0.3%-S	1000	150	0.45	15.05	0.045
	1.0%-S	1000	150	1.50	15.15	0.150
	2.0%-S	1000	150	3.00	15.30	0.300
	3.0%-S	1000	150	4.50	15.45	0.450
NaHCO ₃ (NaHCO ₃ 84.007 g/mol)	0.3%-S	1000	150	0.45	15.05	0.045
	0.5%-S	1000	150	0.75	15.08	0.075
	1.0%-S	1000	150	1.50	15.15	0.150
	1.5%-S	1000	150	2.25	15.23	0.225

Note: For example, 0.3%-S refers to sandy soil with pore liquid concentration of 0.3%.

Table 2. Composition of the pore fluid with single soluble sodium salt

NaCl	$m_{\text{water/g}}$	$m_{\text{NaCl/g}}$	Na ₂ SO ₄	$m_{\text{water/g}}$	$m_{\text{Na}_2\text{SO}_4/\text{g}}$	NaHCO ₃	$m_{\text{water/g}}$	m_{NaHCO_3}
0.3%	150	0.45	0.3%	150	0.45	0.3%	150	0.45
1.0%	150	1.50	1.0%	150	1.50	0.5%	150	0.75
3.5%	150	5.25	2.0%	150	3.00	1.0%	150	1.50
5.0%	150	7.50	3.0%	150	4.50	1.5%	150	2.25

Note: For example, 0.3% refers to a pore fluid with salt concentration of 0.3%.

The soil is of medium compactness ($1/3 < D_r \leq 2/3$). According to the relationship between relative compactness and dry density ($D_r = \frac{\rho_{dmax}(\rho_d - \rho_{dmin})}{\rho_d(\rho_{dmax} - \rho_{dmin})}$), range of the dry density (ρ_d) is 1.64-1.73 g/cm³, and height of the sandy soil is controlled at approximately 6.5 cm. The water content is 15%, and the saturation (S_r) is 71.3%. The configured sandy soil is placed in a fresh-keeping bag for 24 h to mix the water and sand evenly.

The EIS tests are performed under the three-electrode system, with working electrode (WE, the copper sheet of 1 mm×95 mm×120 mm), counter electrode (CE, the copper sheet of 1 mm×95 mm×120 mm) and reference electrode (RE, calomel electrode). Both copper sheets are separately pasted on the opposite faces of a quartz glass cell, and the bonding surface of the WE and CE are sealed by wax to reduce the influence of the working areas on the test. The EIS test is performed using CS350 electrochemical workstation (Wuhan Corrtest Instruments Corp., LTD.) with a sinusoidal AC excitation signal amplitude of 5 mV and a scanning frequency range of 10⁻²-10⁵ Hz. Plastic wrap is used to cover the glass slot during the test, and the temperature is the indoor temperature (20 °C). The salt is weighed on an electronic balance with an accuracy of 0.001, and the others items are weighed on an electronic balance with an accuracy of 0.01.

3. RESULTS AND DISCUSSION

3.1 Equivalent circuit of sandy soil and pore fluid

Adsorption can change the surface state of the electrode and the distribution of the potential in the double layer, thereby affecting the surface concentration of the reaction particles and the activation energy of the interface and directly affecting the electrode process. Figure 3 shows the interface structure of the sandy soil/electrode and clay soil/electrode, which mainly includes the electrical double layer at the electrode-solution interface and the water film at the particle-solution interface [31,32]. At the interface of metal electrode and pore fluid, electrical double layer can be divided into Helmholtz layer and Gouy layer [32].

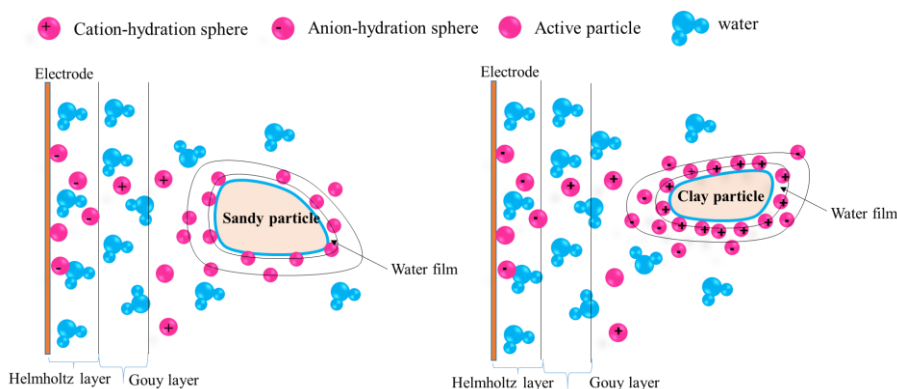


Figure 3. Interface structure of the sandy soil/electrode and clay soil/electrode

There is almost no negatively charged clay particles in the sandy soil, the particles have a weak adsorption effect on the cations, and water film at the sandy particle-solution interface does not have the structure of electrical double layer [31]. The characteristic adsorption on the surface of the sandy particles does not depend on residual charge, and reflects in the capacitance and resistance of sandy layer.

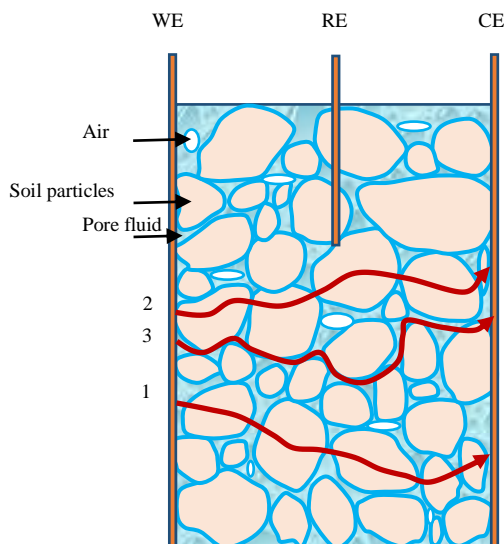


Figure 4. Schematic diagram of the three-electrode system of the sandy soil

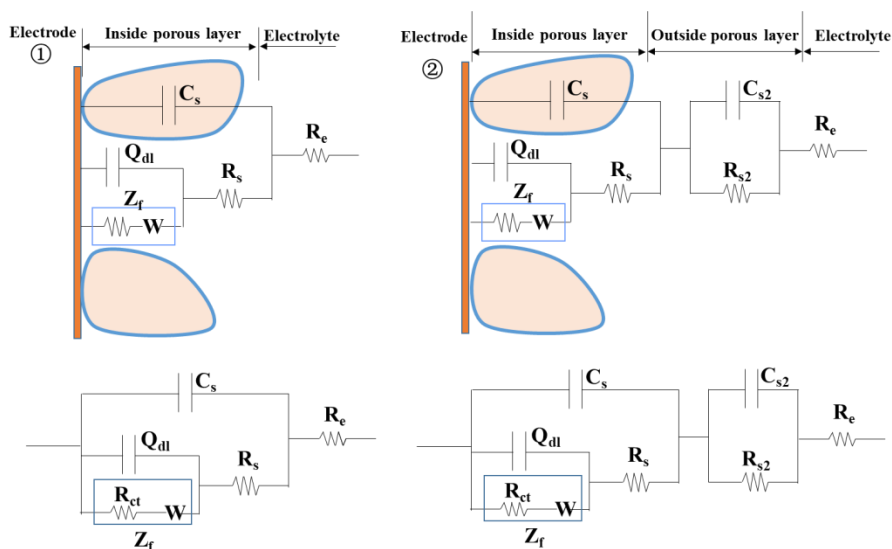


Figure 5. Equivalent circuit of the sandy soil system

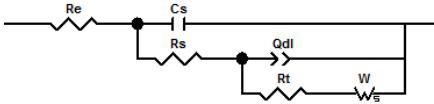
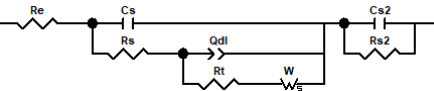
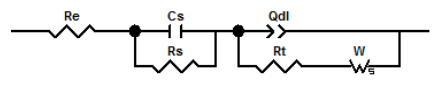
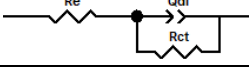
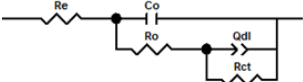
The three-electrode system (Figure 4) consists of two loops, one loop consisting of the working electrode (WE) and reference electrode (RE) for testing the electrochemical reaction process of the working electrode and the other loop consisting of the working electrode (WE) and counter electrode (CE) for transporting electrons. In soil, the current flows through an overall cross-sectional area that is

linked to the saturation level [19]. The conductive path in sand mainly includes the following [33]: 1. a solid-liquid alternating interface formed by discontinuous solid-phase sand particles and pore fluid; 2. a solid-liquid alternating interface formed by continuous solid-phase sand particles and liquid bridge; and 3. a continuous liquid phase between sand particles.

In short, the equivalent circuit of the entire system is simplified to the basic equivalent circuit ① $R(C(R(Q(RW))))$ (Figure 5), where $Q_{dl}(R_{ct}W)$ is the capacitance of electrical double layer and Faradaic resistance formed at the interface of the electrode and pore fluid, (C_sR_s) is the capacitance and resistance of the inner porous layer close to the electrode [34], R_e is the solution resistance, and the capacitance formed by sand adsorption is represented by C_s in sandy soil.

When the amount of stored charge in the sand is large, the equivalent circuit of the system changes. On the one hand, a parallel-composite component $(C_{s2}R_{s2})$ representing the outer sand layer can be added, such as ② $R(C(R(Q(RW))))(CR)$; on the other hand, the connection of circuit elements in the equivalent circuit may also vary with the change in soil properties, such as ③ $R(Q(RW))(CR)$ [35]. In this work, the relative equivalent circuits for different systems are listed in Table 3.

Table 3. Equivalent circuit for different systems

No.	Equivalent circuit	Comment
①	$R(C(R(Q(RW))))$ 	Sandy soil containing low concentration of NaCl (0.3%-S, 1.0%-S); Sandy soil containing NaHCO ₃
②	$R(C(R(Q(RW))))(CR)$ 	Sandy soil containing Na ₂ SO ₄
③	$R(Q(RW))(CR)$ 	Sandy soil containing high concentration of NaCl (3.5%-S, 5.0%-S)
④	$R(QR)$ 	NaCl and Na ₂ SO ₄ pore fluid
⑤	$R(C(R(QR)))$ 	NaHCO ₃ pore fluid

For sandy soil systems, the basic components of the equivalent circuit are the solution resistance R_e , resistance and capacitance of sand layer $(C_s, R_s$ and $C_{s2}, R_{s2})$ and the capacitance of electrical double layer and Faradaic resistance $Q_{dl}(R_{ct}W)$ formed at the interface of the electrode and pore liquid. The equivalent circuit ① is a basic equivalent circuit, and other equivalent circuits are all extensions.

The variation of the equivalent circuit is related to the concentration and type of ions in each contaminated sandy soil. The basic equivalent circuits for the salt solution system are ③ and ⑤. In sandy soil, the mobility and aggression of Cl^- are high, the charge of SO_4^{2-} is high and HCO_3^- contributes to the formation of oxide on the surface of the electrode. The selection of the specific equivalent circuit is debugged according to the characteristics of the corresponding system and the test

results of the electrochemical impedance spectrum. For the solution system, the corresponding equivalent circuit is selected based on the basic equivalent circuit models $R(QR)$ and $R(C(R(QR)))$ and the characteristics of the liquid phase environment. R_{ct} is a charge transfer resistor, and Q_{dl} is a constant phase element.

3.2 Electrochemical characteristics of sandy soil containing NaCl

Figure 6 is the Nyquist diagram of sandy soil and pore fluids containing different contents of NaCl. For an environment with mobile and aggressive ion (Cl^-), the Nyquist diagram consists of a capacitive loop connected to a nearly 45° line (diffusion impedance). With increasing NaCl concentration, the radius of the capacitive loop decreases, and the corrosivity of sandy soil and pore fluid increases.

It is obvious that the sand particles cause the intersection of the impedance spectrum and the real axis to move to the right, which is related to the discontinuity of the interface impedance of the working electrode [29, 36]. Compared with the pore fluid, the capacitive loop of sandy soil with NaCl presents a smaller radius and the length of the slash of nearly 45° (diffusion resistance) is small.

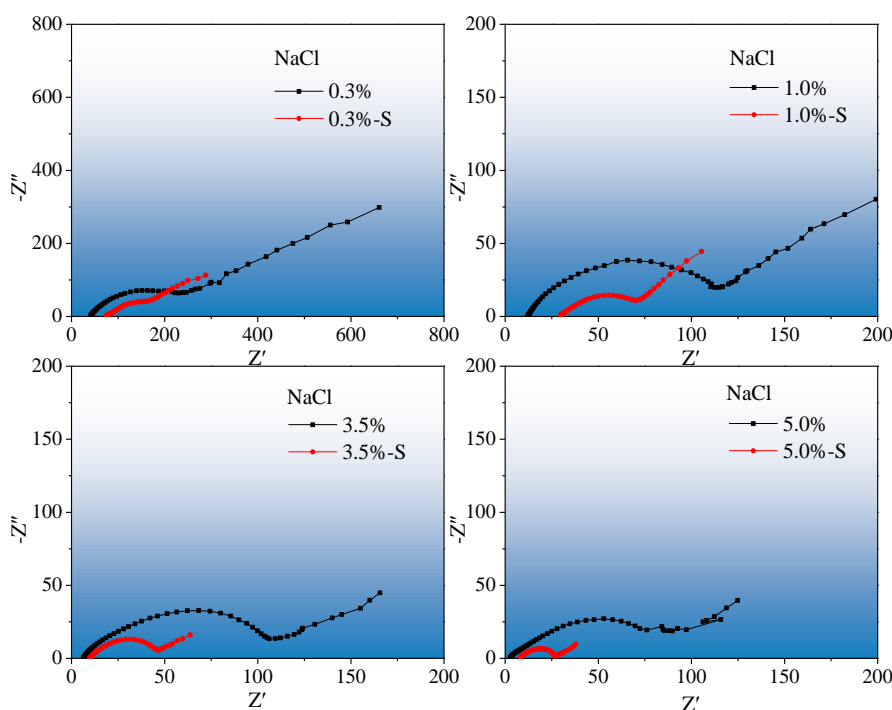


Figure 6. Nyquist diagram of sandy soil and pore fluid containing NaCl

Figures 7-8 show the Bode diagram of the sandy soil and pore fluid containing NaCl (modulus and phase angle diagrams, respectively). The modulus of the sandy soil and the modulus of the pore fluid intersect in the interval of $10^0 \sim 10^3$ Hz. The porous structure of sandy soil promotes low frequency processes and hinders high frequency processes. The peaks of phase angle for sandy soil

containing NaCl is lower than that of pore fluid containing NaCl, and the peak value moves towards the low frequency region. This result reflects that the sandy soil is more corrosive than the pore fluid [37]. With increasing NaCl concentration, the peaks and valleys of phase angle for sandy soil containing NaCl are more obvious, which also reflects the enhanced corrosivity of sandy soil.

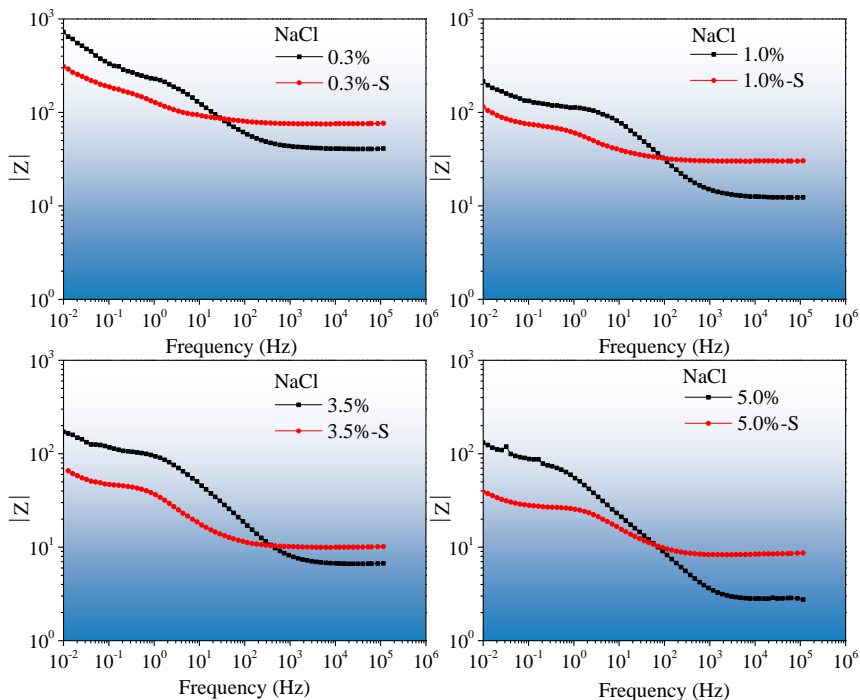


Figure 7. Bode diagram (modulus value) of sandy soil and pore fluid containing NaCl

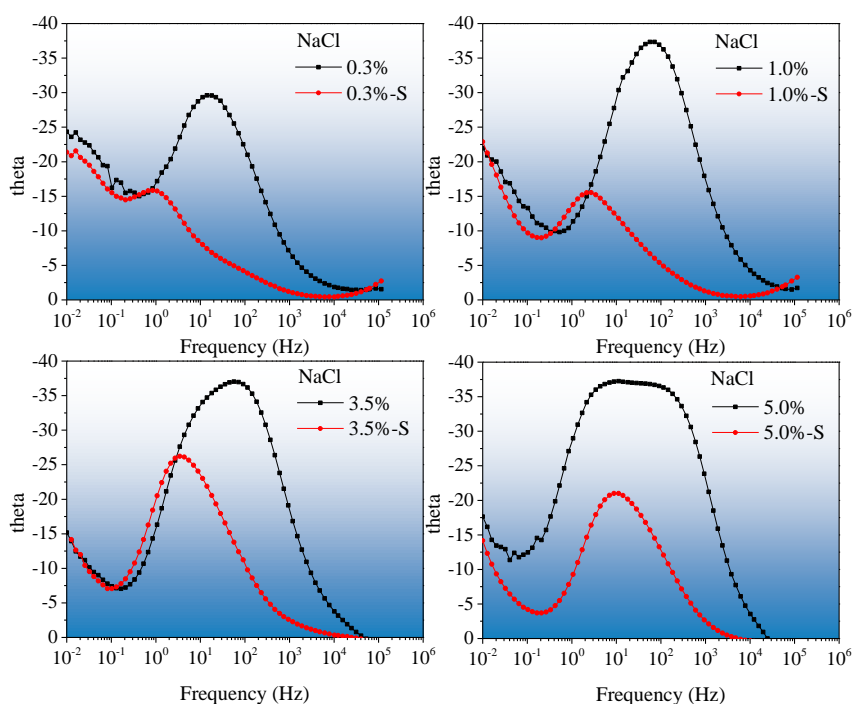


Figure 8. Bode diagram (phase angle) of sandy soil and pore fluid containing NaCl

For further research, equivalent circuits ① $R(C(R(Q(RW))))$ and ③ $R(Q(RW))(CR)$ are used to fit the impedance spectra of sandy soils containing low concentrations (0.3% and 1.0%) and high concentrations (3.5% and 5.0%) of NaCl, respectively. The results are shown in Table 4. The fitting software ZSimDemo3.30 is used. The high frequency regions of pore fluids with different concentrations of NaCl are fitted by equivalent circuit ④ $R(QR)$. The fitting software Zview2 is used, and the results are shown in Table 5.

Table 4. EIS fitting results of sandy soil containing different concentrations of NaCl

Sample	$R_e (\Omega \cdot \text{cm}^2)$	$R_{ct} (\Omega \cdot \text{cm}^2)$	Q_{dl}		$C_s (\text{F} \cdot \text{cm}^{-2})$	$R_s (\Omega \cdot \text{cm}^2)$	$W (\text{S} \cdot \text{s}^{0.5} \cdot \text{cm}^{-2})$
			$Y_o (\text{S} \cdot \text{s}^{-n} \cdot \text{cm}^{-2})$	n			
0.3%-S	76.56	92.22	3.29E-3	0.71	1.37E-4	11.20	0.023
1.0%-S	30.25	26.61	2.81E-3	0.88	3.58E-4	7.79	0.073
3.5%-S	9.891	17.50	5.03E-3	0.69	7.46E-4	16.01	0.188
5.0%-S	8.406	13.10	6.65E-3	0.73	7.26E-4	4.18	0.310

Table 5. EIS fitting results of different concentrations of NaCl pore fluid

Sample	$R_e (\Omega \cdot \text{cm}^2)$	Error%	Q_{dl}				$R_{ct} (\Omega \cdot \text{cm}^2)$	Error%
			$Y_o (\text{S} \cdot \text{s}^{-n} \cdot \text{cm}^{-2})$	Error%	n	Error%		
0.3%	39.89	0.33	5.75E-4	2.18	0.64	0.65	259.9	1.22
1.0%	11.23	1.75	5.38E-4	4.38	0.67	1.14	122.9	1.82
3.5%	5.503	1.78	1.32E-3	2.08	0.61	0.66	117.5	1.01
5.0%	2.560	1.45	3.79E-3	3.75	0.58	1.15	103.0	2.96

The results show that the R_e and R_{ct} of sandy soil containing NaCl decrease with increasing concentration. The R_e of sandy soils is approximately 2-3 times that of the corresponding pore fluid, but the R_{ct} of sandy soils is relatively small. This result is consistent with the results of the Nyquist and Bode diagrams. In addition, the capacitance and resistance of the complex sand layer fluctuate to a certain degree in the sandy soil, and there is a diffusion impedance (W). The values of n show that there is a deviation between the interface capacitance and the ideal capacitance, and the parameter Y_o of the constant phase element is on the order of 10^{-3} for the sandy soil, which is larger than that for the pore fluid.

3.3 Electrochemical characteristics of sandy soil containing Na_2SO_4

Figure 9 is the Nyquist diagram of sandy soil and pore fluid containing Na_2SO_4 . In the SO_4^{2-} environment with a large amount of charge, the Nyquist diagram presents a flat capacitive loop. Fluctuations occur at the low frequency end for the pore fluid system, and the fluctuations are minimal at high concentrations of Na_2SO_4 . Obviously, the capacitive loop of sandy soil containing Na_2SO_4 has

a smaller radius than that of the Na_2SO_4 solution, showing a large corrosivity. On the whole, a change in the Na_2SO_4 concentration has minimal effects on the capacitive loop and corrosivity of the sandy soil.

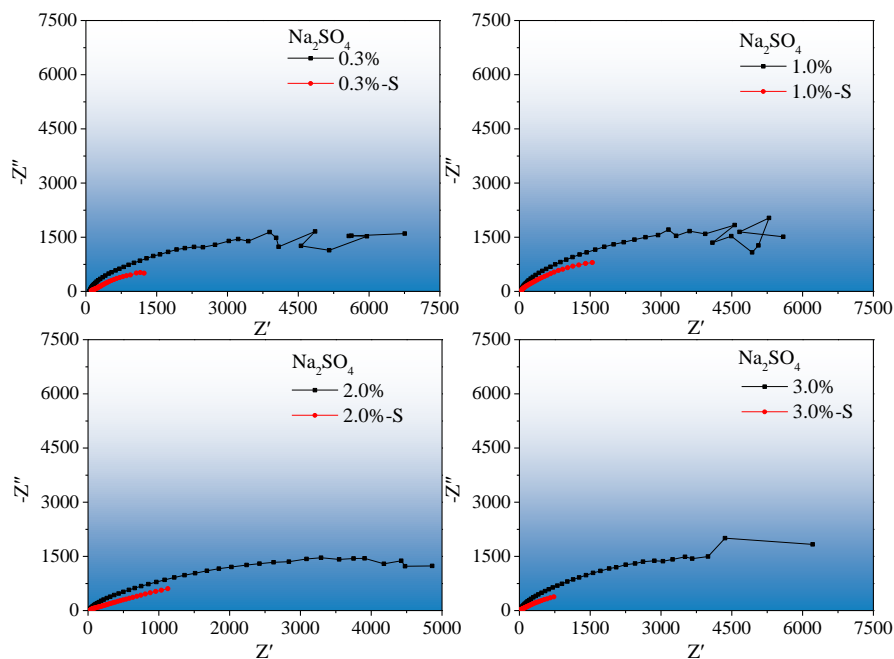


Figure 9. Nyquist diagram of sandy soil and pore fluid containing Na_2SO_4

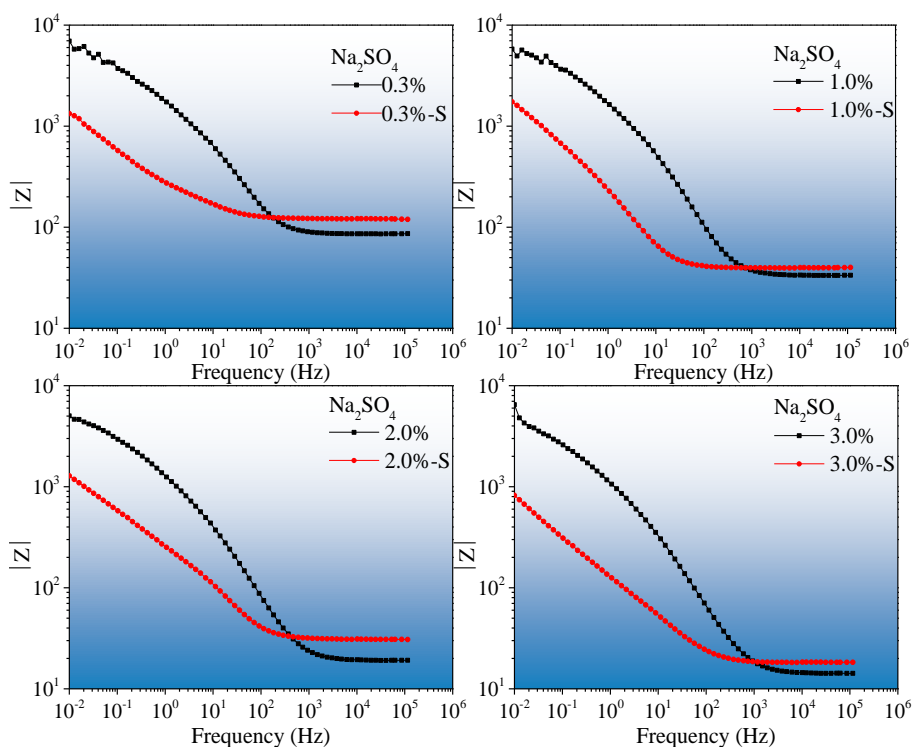


Figure 10. Bode diagram (modulus value) of sandy soil and pore fluid containing Na_2SO_4

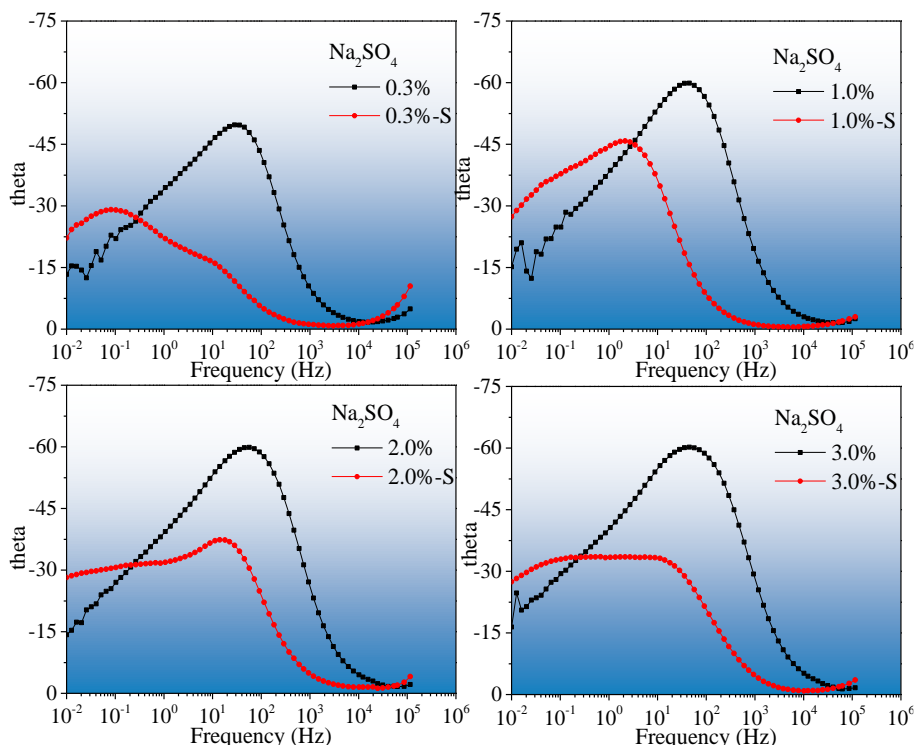


Figure 11. Bode diagram (phase angle) of sandy soil and pore fluid containing Na₂SO₄

Figures 10-11 show the Bode diagram of the sandy soil and pore fluid containing Na₂SO₄ (modulus and phase angle, respectively). The Bode diagram shows that the modulus of the sandy soil and that of the pore fluid also cross between frequencies of 10⁰~10³ Hz, and the intersection moves towards 10³ Hz as the salt concentration increases. Similarly, the sand particles play a role in facilitating the low frequency process and hindering the high frequency process. However, the low-frequency boosting effect is more significant than the high-frequency blocking effect. The phase angle of sandy soil presents two peaks, indicating that the impedance spectrum contains two time-constants caused by state variables, which may be related to the adsorption state of the ions in sandy soil with a porous structure. The peak of phase angle for the sandy soil is lower than that of the pore fluid, which shows the strong corrosivity of sandy soil containing Na₂SO₄ [37].

In the sand, SO₄²⁻ with a large amount of charge is dispersed in the pore liquid around the sand particles and exists in the form of a “liquid bridge”. Therefore, the equivalent circuit ② R(C(R(Q(RW))))(CR) is used to fit the impedance spectrum of sandy soil containing Na₂SO₄, which forms by connecting the composite circuit component ((RC), representing the outer sand layer) in series with circuit ① R(C(R(Q(RW))))). The results are shown in Table 6, and the fitting software ZSimDemo3.30 is used. The fitting results of the high-frequency impedance spectrum of the pore fluid by equivalent circuit ④ are shown in Table 7, and the fitting software Zview2 is used.

The results show that with increasing Na₂SO₄ concentration, the solution resistance (R_e) for the sandy soil gradually decreases, and the charge transfer resistance (R_{ct}) fluctuates slightly. The R_e for sandy soil is approximately twice that of the pore fluid, but the R_{ct} is relatively small. This result is consistent with the results of the Nyquist and Bode diagrams. In addition, the capacitance and resistance of the sand layer fluctuate to a certain degree, and the fluctuation of the outer sand layer is

large. From n , it is known that there is a deviation between the interface capacitance and the ideal capacitance, and the Y_o of the constant phase element for the sandy soil is on the order of 10^{-3} , which is larger than that for the pore fluid (10^{-5}).

Table 6. EIS fitting results of sandy soil containing different concentrations of Na_2SO_4

Samples	R_e ($\Omega \cdot \text{cm}^2$)	$R_{ct}(\Omega \cdot \text{cm}^2)$	Q_{dl}		C_s ($\text{F} \cdot \text{cm}^2$)	R_s ($\Omega \cdot \text{cm}^2$)	W ($\text{S} \cdot \text{s}^{-0.5} \cdot \text{cm}^2$)	C_{s2} ($\text{F} \cdot \text{cm}^2$)	R_{s2} ($\Omega \cdot \text{cm}^2$)
			Y_o ($\text{S} \cdot \text{s}^{-n} \cdot \text{cm}^2$)	n					
0.3%-S	122.7	1.22E3	2.40E-3	0.52	1.2E-4	48.86	2.3E10	2.4E-2	443.8
1.0%-S	39.77	2.10E3	1.47E-3	0.48	2.3E-4	1.5E-3	1.5E5	2.2E-2	678.6
2.0%-S	31.37	5.31E3	2.02E-3	0.40	6.6E-5	5.4E-5	3.3E-2	9.5E-4	19.87
3.0%-S	18.29	1.06E3	3.49E-3	0.44	9.6E-5	1.433	1.3E5	4.2E-2	295.8

Table 7. EIS fitting results of different concentrations of Na_2SO_4 pore fluid

Samples	$R_e(\Omega \cdot \text{cm}^2)$	Error%	Q_{dl}				$R_{ct}(\Omega \cdot \text{cm}^2)$	Error%
			$Y_o(\text{S} \cdot \text{s}^{-n} \cdot \text{cm}^2)$	Error%	n	Error%		
0.3%	67.58	3.64	6.82E-5	4.80	0.74	1.29	2106	4.79
1.0%	24.93	5.34	6.76E-5	3.75	0.78	0.92	2038	4.34
2.0%	14.86	4.13	9.19E-5	3.27	0.77	0.76	1564	4.13
3.0%	11.43	3.15	11.79E-5	2.35	0.76	0.55	1468	3.47

3.4 Electrochemical characteristics of sandy soil containing NaHCO_3

Figure 12 shows the Nyquist diagram of sandy soil and pore fluid containing NaHCO_3 . In the environment with HCO_3^- , which contributes to the formation of a passivation film on the steel surface, the Nyquist patterns exhibit a flat capacitive loop. The radius of the capacitive loop for the sandy soil is slightly smaller than that for the pore fluid, showing the large corrosivity of the sandy soil. Overall, a change in NaHCO_3 concentration has little effect on the corrosivity of the sandy soil and pore fluid, and an NaHCO_3 concentration of 0.3% corresponds to the largest impedance spectrum radius, which may be related to the properties of the pore fluid.

Figures 13-14 show the Bode diagram of the sandy soil and pore fluid containing NaHCO_3 (modulus and phase angle, respectively). The modulus of the sandy soil containing NaHCO_3 and that of pore fluid containing NaHCO_3 also cross between frequencies of $10^0 \sim 10^3$ Hz. Similarly, the sand particles play a role in promoting the low-frequency process and hindering the high-frequency process, and the low-frequency promotion is more significant than the high-frequency barrier. The peak of phase angle for the sandy soil is lower than that of the pore fluid, which shows that sandy soil with NaHCO_3 is more corrosive than pore fluid [37]. The phase angles of sandy soil and pore fluid with NaHCO_3 both have two peaks (in particular for sandy soil), indicating that the impedance spectrum contains two time-constants caused by state variables.

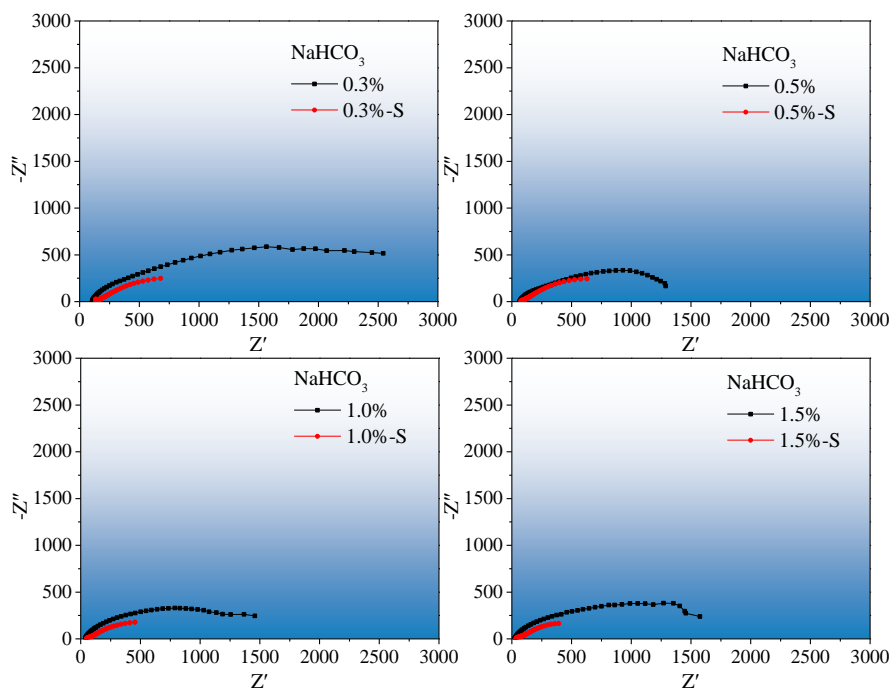


Figure 12. Nyquist diagram of sandy soil and pore fluid containing NaHCO_3

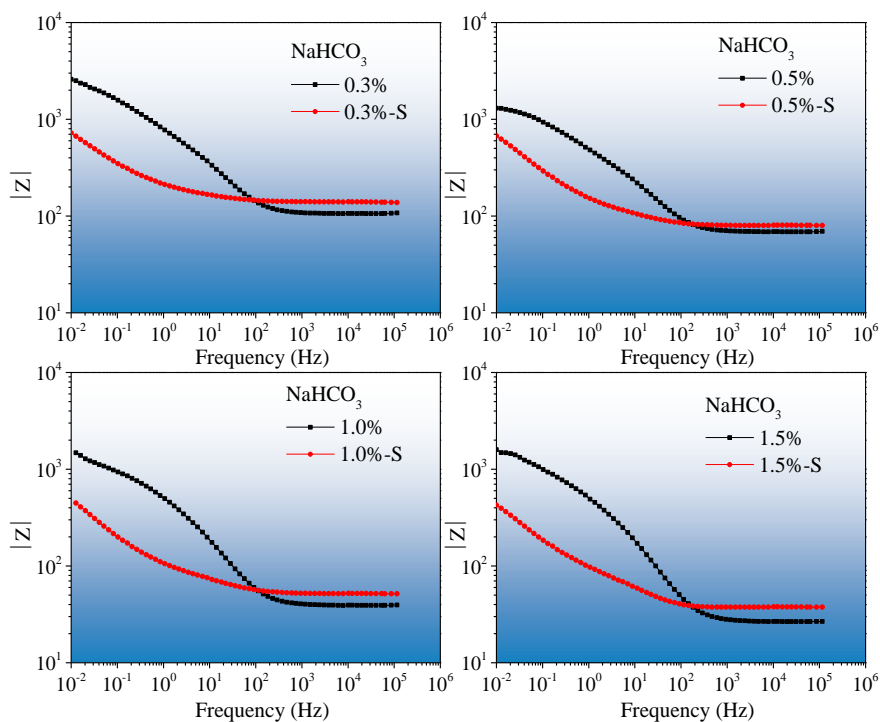


Figure 13. Bode diagram (modulus value) of sandy soil and pore fluid containing NaHCO_3

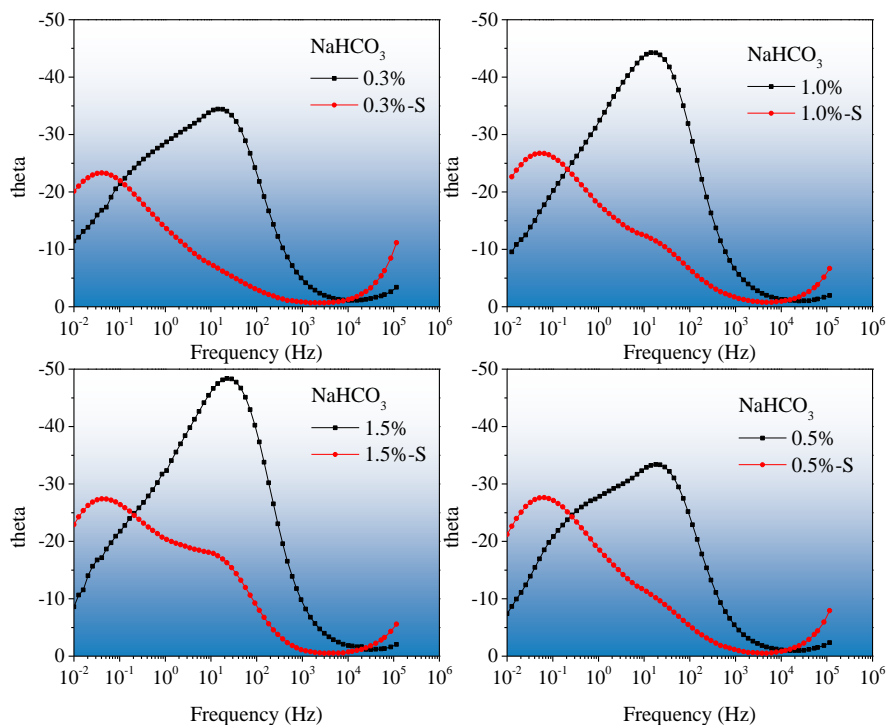


Figure 14. Bode diagram (phase angle) of sandy soil and pore fluid containing NaHCO₃

Similarly, the equivalent circuit (1) $R(C(R(Q(RW))))$ is used to fit the impedance spectrum of sandy soil containing NaHCO₃. The impedance spectra of different concentrations of NaHCO₃ pore fluid are fitted by equivalent circuit (5) $R(C(R(QR)))$ without diffusion impedance (W), as shown in Table 3. C_o and R_o in the equivalent circuit (5) for the pore fluid represent the capacitance and resistance of the passivation film on the working electrode surface, respectively. The porous interface in the sandy soil with NaHCO₃ means a continuous passivation film cannot be formed on the surface of the working electrode. C_s and R_s in the equivalent circuit (1) for the sandy soil represent the resistance and capacitance of the sand layer near the working electrode, respectively. The fitting software ZSimDemo3.30 is used, and the results are shown in Tables 8-9.

Table 8. EIS fitting results of sandy soil containing different concentrations of NaHCO₃

Samples	R _e (Ω·cm ²)	R _{ct} (Ω·cm ²)	Q _{dl}		C _s (F·cm ⁻²)	R _s (Ω·cm ²)	W (S·s ^{0.5} ·cm ⁻²)
			Y _o (S·s ⁻ⁿ ·cm ⁻²)	n			
0.3%-S	135.3	1516	4.59E-3	0.46	1.93E-9	138.8	1.12E11
0.5%-S	79.03	1071	5.04E-3	0.55	1.63E-4	23.42	2.81E5
1.0%-S	51.29	771.6	7.38E-3	0.55	1.89E-4	19.86	9.99E8
1.5%-S	37.44	912.5	7.73E-3	0.49	2.43E-4	21.91	3.74E6

Table 9. EIS fitting results of different concentrations of NaHCO₃pore fluid

Samples	R _e (Ω·cm ²)	R _{ct} (Ω·cm ²)	Q _{dl}		C _o (F·cm ⁻²)	R _o (Ω·cm ²)
			Y _o (S·s ⁻ⁿ ·cm ⁻²)	n		
0.3%	107.4	39.83	5.65E-4	0.42	1.875E-5	3434
0.5%	69.48	56.83	8.41E-4	0.47	2.897E-5	1571
1.0%	39.54	1.36E-3	6.87E-4	0.44	3.625E-5	1739
1.5%	26.94	1.58E-4	6.72E-4	0.43	3.486E-5	2073

The fitting results show that the solution resistance (R_e) for the sandy soil decreases with increasing of NaHCO₃ concentration, and the charge transfer resistance (R_{ct}) tends to be stable with increasing concentration. The difference between the R_e of the sandy soil and the pore fluid system is small, but the difference between their R_{ct} is significant. This result is consistent with the results of the Nyquist and Bode diagrams. In addition, the capacitance and resistance of the sand layer fluctuate to a certain degree, but the capacitance and resistance of the passivation film are relatively stable. It can be seen from n that there is deviation between the interface capacitance and the ideal capacitance, and the parameter Y_o of the constant phase element for the sandy soil is on the order of 10⁻³, which is larger than that (10⁻⁴) for the pore fluid.

3.5 Mechanism of pore fluid and sand particles

Under the disturbance of a small amplitude sinusoidal alternating wave signal, the electrochemical reactions that may occur in sandy soil containing Na₂SO₄ include the copper electrode oxidation process (anode, formula (1)) and oxygen reduction process (cathode, formula (2)). In addition, the free ions in the pore fluid move in the vicinity of the sand-electrode interface to form an electrical double layer (Figure 2).

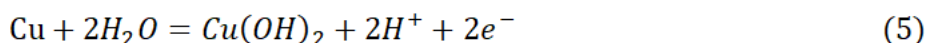


In neutral-sandy soil containing NaCl, a dense CuCl crystal covering layer can be formed on the noninert electrode copper [38, 39]:



As the Cl⁻ concentration increases, the dissolution of copper is more likely to occur.

In sandy soil with NaHCO₃, there are Cu(OH)₂ and CuOH formed on the anode, which then are decomposed into CuO and Cu₂O layer, and CuO is the main product [40-42]. The electrochemical process is weakened when a dense oxide layer is formed.



In general, sandy soils containing NaHCO_3 are less corrosive and has a certain protective effect on copper electrodes. While the sandy soils containing NaCl and Na_2SO_4 are more corrosive, and the environment containing NaCl is the most corrosive.

As shown in Figure 15, the electrochemical reaction area of the working electrode (copper) under the droplet can be divided into the "TPB (three-phase boundary) region" and "bulk region" (the centre of the droplet) [43, 44]. The electrolyte layer of the ring-shaped "TPB region" is smaller than $100\ \mu\text{m}$, and the electrolyte layer in the "bulk region" is greater than $100\ \mu\text{m}$ thick. Here, the "TPB region" acts as the cathode, and the "bulk region" is the anode.

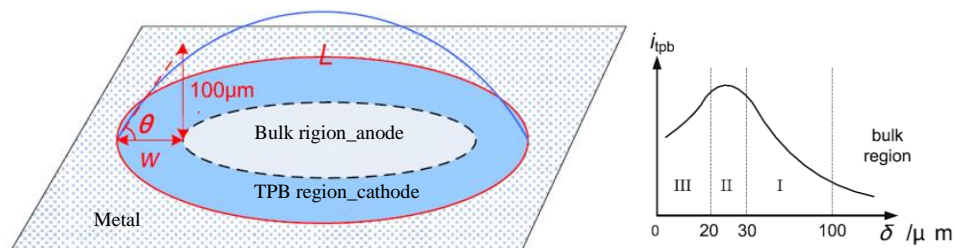


Figure 15. Geometry of electrolyte droplets adsorbed on a flat electrode

The sand particles facilitate low-frequency processes and hinder high-frequency processes. In the high frequency region, the three conductive paths in the sand are mostly in the conducting state, the corresponding electrochemical process is hindered by the sand particles, and the corresponding modulus is large. In the low frequency region, the liquid phase conductive path plays a dominant role in the sandy soil, while the sand particles have a dispersion effect on the pore fluid, so the corresponding modulus value for the sand system is small [35].

Compared to pore fluid, the sandy soil system has a small peak, and the peak appears in a higher frequency domain. At frequencies of $10^0\sim 10^2$ Hz, the peak of phase angle for sandy soil containing NaCl , Na_2SO_4 or NaHCO_3 is greatly affected by a change in the concentration of sodium salt, which may be caused by the porous structure consisting of the sand particles and the state of the "liquid bridge"[45] surrounding the sand particles related to the conductive path in the system.

Overall, the corrosivity of sandy soil is stronger than that of pore fluid. The sufficient oxygen in the sand system with solid, liquid and gas three-phase structures promote the electrochemical process. In addition, the adsorption of sand particles with water and ions forms a large number of micro capacitors and current path networks, which also promotes the electrochemical process [29, 36]. However, the passivation of the electrode surface prevents the electrochemical process from proceeding [32]. In the alkaline environment, a partial active area of the sand-electrode interface is covered by the oxidation product, and the area not covered by the oxidation product is dissolved as the anode. This process is more likely to occur in the sand systems containing high-concentration NaHCO_3 , and thus, the radius of resistance and modulus are small.

4. CONCLUSIONS

In this work, EIS tests and comprehensive analyses were carried out for sandy soil and pore fluids containing various soluble sodium salts (NaCl, Na₂SO₄ or NaHCO₃). The effect of pore fluid and sand particles on the electrochemical characteristics of sandy soil containing soluble sodium salt was explored. The results are as follows:

(1) An electrochemical microbattery is formed in the interface region of the pore fluid and the working electrode. The basic equivalent circuit of the sandy soil system is circuit ① $R(C(R(Q(RW))))$. The equivalent circuits of the sandy soil containing NaCl, Na₂SO₄ and NaHCO₃ are slightly different, changing with the discrepancy in the properties and concentration of soluble sodium salt.

(2) The electrochemical impedance spectra of the sandy soil containing NaCl, Na₂SO₄ and NaHCO₃ possesses their own characteristics. The Nyquist diagram of sandy soil containing NaCl is composed of a capacitive loop and diffusion impedance (the nearly 45° oblique line) and that of sandy soil with Na₂SO₄ and NaHCO₃ is a flat capacitive loop.

(3) A change in sodium salt concentration has the greatest effect on the electrochemical behaviour of the environment containing NaCl, which is related to properties of anions. At frequencies of 10⁰~10² Hz, the peak of phase angle for the sandy soil containing NaCl, Na₂SO₄ or NaHCO₃ is greatly affected by the concentration, which may be caused by the porous structure and the state of the "liquid bridge".

(4) Compared with the pore fluid system, the radius of the capacitive loop and the peak of phase angle for the sandy soil is small, showing the high corrosivity of the sandy soil. The phase angles of the sandy soil with Na₂SO₄ or NaHCO₃ and the NaHCO₃ pore fluid show two peaks, which may be related to the adsorption state of the ions in the porous structure of the sandy soil and the passivation of the electrode surface.

(5) The sand particles facilitate low-frequency processes and hinder high-frequency processes. In the high frequency region, the three conductive paths in the sandy soil are mostly in the conducting state, and the corresponding modulus is large. In the low frequency region, the liquid phase conductive path plays a dominant role in the sandy soil, so the corresponding modulus value for the sand system is small.

ACKNOWLEDGMENTS

The authors would like to express their gratitude to the funding provided by "1331" Innovation Team of Jinzhong University (jzycxtd2019008), PhD research launch project of Jinzhong University, National Natural Science Foundation of China (No. 51208333, No. 41807256), Program for the Outstanding Innovative Teams of Higher Learning Institutions of Shanxi (No.OIT2015), State Key Laboratory of Geomechanics and Geotechnical Engineering, Institute of Rock and Soil Mechanics, Chinese Academy of Sciences (No. Z017003) and Key Laboratory of Ministry of Education for Geomechanics and Embankment Engineering, Hohai University (No. 201702).

References

1. L. M. Quej-Ake, and A. Contreras, *Anti-Corros. Methods Mater.*, 65 (2018) 97.
2. N. M. Lin, J. J. Zou, Z. X. Wang, Y. Ma, W. Tian, X. F. Yao, L. Qin, Z. H. Wang, and B. Tang, *Rare Met. Mater. Eng.*, 47 (2018) 274.
3. N. M. Lin, P. Zhou, J. J. Zou, F. Q. Xie, and B. Tang, *J. Wuhan Univ. Technol.*, 30 (2015) 622.
4. Z. Y. Liu, Q. Li, Z. Y. Cui, W. Wu, Z. Li, C. W. Du, and X. G. Li, *Constr. Build. Mater.*, 148 (2017) 131.
5. B. Wang, X. X. Guo, H. Jin, F. H. Li, and Y. Song, *Constr. Build. Mater.*, 214 (2019) 37.
6. C. N. Cao, Natural environmental corrosion of Chinese materials, *Chemical Industry Press*, (2005) Beijing, China.
7. P. Victor, G. Pouria, and A. Akram, *Constr. Build. Mater.*, 40 (2013) 908.
8. S. Claudia, and A. Akram, *Constr. Build. Mater.*, 102 (2016) 904.
9. X. R. Li, Z. X. Yao, and Z. B. Cao, *Rock Soil Mech.*, 25 (2004) 1229.
10. C. P. Zhu, and H. L. Liu, *Rock Soil Mech.*, 28 (2007) 625.
11. X. Y. Wang, P. J. Han, X. H. Bai, and X. Y. Li, *Constr. Build. Mater.*, 205 (2019) 511.
12. W. M. Ye, W. Huang, B. Chen, C. Yu, and J. Wang, *Rock Soil Mech.*, 30 (2009) 1899.
13. Q. Liu, X. L. Zheng, J. G. Ren, J. G. Wang, X. H. Zhang, and G. Q. Lin, *Mar. Environ. Sci.*, 27 (2008) 443.
14. H. Farrah, and W. F. Pickering, *Water Air Soil Pollut.*, 8 (1977) 189.
15. P. K., and P. W. F., *Water Air Soil Pollut.*, 5 (1975) 63.
16. H. X. Wan, X. J. Yang, Z. Y. Liu, D. D. Song, C. W. Du, and X. G. Li, *J. Mater. Eng. Perform.*, 26 (2017) 715.
17. W. Wei, X. Q. Wu, W. Ke, S. Xu, B. Feng, and B. T. Hu, *J. Mater. Eng. Perform.*, 26 (2017) 4340.
18. I. Ibrahim, M. Meyer, H. Takenouti, and B. Tribollet, *J. Braz. Chem. Soc.*, (2017).
19. R. Akkouche, C. Rémazeilles, M. Barbalat, R. Sabot, M. Jeannin, and P. Refait, *J. Electrochem. Soc.*, 164 (2017) C626.
20. M. R. Wang, and P. J. Han, *Sci. Technol. Eng.*, 18 (2018) 90.
21. Y. Hao, P. J. Han, and B. He, *Sci. Technol. Eng.*, 18 (2018) 106.
22. X. Y. Wang, P. J. Han, and Q. Zhang, *Sci. Technol. Eng.*, 16 (2016) 255.
23. X. L. Zhang, Y. F. Zhang, and P. J. Han, *Sci. Technol. Eng.*, 16 (2016) 16.
24. J. Jiang. The role of liquid dispersion in gas/liquid/solid multiphase corrosion systems. *Ocean University of China*, Shandong, 2009.
25. Y. F. Zhang, P. J. Han, and B. He, *J. Taiyuan Univ. Technol.*, 48 (2017) 55.
26. S. Q. Xu, R. Z. Xie, and P. J. Han, *Sci. Technol. Eng.*, 18 (2018) 100.
27. F. L. Mi, R. Z. Xie, and P. J. Han, *Sci. Technol. Eng.*, 18 (2018) 148.
28. F. L. Ma, R. Z. Xie, P. J. Han, and X. H. Bai, *Int J Electrochem Sc*, 13 (2018) 5396.
29. B. He, P. J. Han, L. F. Hou, D. C. Zhang, and X. H. Bai, *Eng Fail Anal*, 80 (2017) 325.
30. H. Z. Xiao, F. Xie, M. Wu, D. Wang, W. Zhao, and X. H. Luo, *Mater. Prot.*, 50 (2017) 14.
31. L. Q. Ren, *Soil Adhesion Mechanics*, China Machine Press, (2011) Beijing, China.
32. J. Q. Zhang, *Electrochemical Measurement Technology*, Chemical Industry Press, (2010) Beijing, China.
33. B. He. The influence of particle size on the electrochemical corrosion behavior of the contaminated system and X70 steel in NaCl contaminated sandy environment. *Taiyuan University of Technology*, Taiyuan, 2016.
34. P. J. Han, Y. F. Zhang, F. Y. Chen, and X. H. Bai, *J. Cent. South Univ.*, 22 (2015) 4318.
35. M. E. Orazem, and B. Tribollet, *Electrochemical Impedance Spectroscopy*, Chemical Industry Press, (2014) Beijing, China.
36. B. He, X. H. Bai, L. F. Hou, D. C. Zhang, and P. J. Han, *Mater. Corros.*, 68 (2017) 846.
37. Y. X. Guo. Preparation and Properties of SiO₂ based sol-gel Anticorrosion Coatings on Magnesium

- Alloy. Taiyuan University of Technology, Taiyuan, 2017.
38. H. Cui, C. Y. Tan, Y. Zhen, and T. He, *J. Cent. South Univ.*, 42 (2011) 3336.
 39. Y. Raghupathy, K. Anshul, M.Y. Rekha, N.P., Narasimha Rao, and S. Chandan, *Thin Solid Films*, 636 (2017) 107.
 40. Q. Ran, L. Jiang, and D. C. Cai, *J. Sichuan Teach. College*, 11 (1990) 147.
 41. J. B. He, and J. X. Lin, *Chem. J. Chin. Univ.*, 17 (1996) 290.
 42. O. Maité, A. R. Martín, and B. F. Silvia, *Procedia Mater. Sci.*, 9 (2015) 460.
 43. J. Jiang, and J. Wang, *J. Solid State Electrochem.*, 13(2009) 1723.
 44. R. Akkouche, C. Rémazeilles, M. Barbalat, R. Sabot, M. Jeannin, and Ph. Refait, *J. Electrochem. Soc.*, 164(2017) C626.
 45. N. Lu, W. J. Likos, C. F. Wei, L. Hou, and W. X. Jian, *Unsaturated Soil Mechanics*, Higher Education Press, (2012) Beijing, China

© 2020 The Authors. Published by ESG (www.electrochemsci.org). This article is an open access article distributed under the terms and conditions of the Creative Commons Attribution license (<http://creativecommons.org/licenses/by/4.0/>).